IPPK-1 and IP6 contribute to ventral nerve cord assembly in *C. elegans*

Nathaniel Noblett,[1,2] Tony Roenspies,[1] Stephane Flibotte,[4] and Antonio Colavita[1,2,3]

[1]Neuroscience Program, Ottawa Hospital Research Institute, Ottawa, Canada

[2]Department of Cellular and Molecular Medicine, University of Ottawa, Ottawa, Canada

[3]University of Ottawa Brain and Mind Research Institute, Ottawa, Canada

[4]UBC/LSI Bioinformatics Facility, University of British Columbia, Vancouver, Canada

Highlights

- *ipmk-1* and *ippk-1* mutants display neuron position defects in the ventral nerve cord (VNC).
- ippk-1 mutants display disorganization in VNC neuronal precursors during midline convergence.
- IPPK-1 is involved in convergent extension during VNC formation.
- Exogenous IP6 rescues larval and embryonic defects in *ippk-1* mutants.

ABSTRACT

Inositol phosphates (IPs) play important roles in nervous system development and function. One of these roles uncovered by loss-of-function studies, is that IP isomers are essential for proper neural tube formation. In this study, we show that inositol pentakisphosphate 2-kinase (IPPK-1), the kinase that phosphorylates IP5 to generate IP6, is involved in assembling the ventral nerve cord (VNC) in *C. elegans*. We show that mutations in *ippk-1* lead to the mispositioning of motor neurons along the VNC of newly hatched larvae. These positioning defects reflect disruption of VNC assembly during embryogenesis, as *ippk-1* embryos display improper alignment of VNC neuroblasts and delays in rosette-mediated convergent extension (CE). We further show that injection of exogenous IP6 into the gonads of *ippk-1* mutants can rescue both embryonic and neuron positioning defects. Our findings indicate that inositol metabolism is important for regulating CE in *C. elegans* and suggest that IP isomers play a conserved role in the formation of central nerve cords.

Keywords

Convergent extension, nerve cord, inositol phosphate, IPPK

INTRODUCTION

Inositol phosphates and polyphosphates, groups of metabolites produced through the progressive phosphorylation of inositol triphosphate (IP3), are central players in a diverse variety

of cellular roles, including regulating ion channel function, cell migration, exocytosis, developmental timing and establishing left-right asymmetry (Efanov et al., 1997; Yang et al., 2001; Sarmah et al., 2005; Jadav et al., 2016; Yang et al., 2021; Rao et al., 2015). These roles are critical for proper embryogenesis and organogenesis during development (Yang et al., 2021; Frederick et al., 2005; Boitano et al., 1992; Seeds et al., 2015). In the developing nervous system, the activity of inositol phosphate and polyphosphate kinases regulate several aspects of brain development and post-development nervous system function (Loss et al., 2013; Park et al., 2019a; Park et al., 2019b; Ahmed et al., 2015; Wilson et al., 2009). Regulation of inositol phosphate levels, specifically inositol pentakisphosphate (IP5) and inositol hexaphosphate (IP6), are important for neuronal survival and differentiation (Loss et al., 2013; Ucuncu et al., 2020). Additionally, loss of inositol hexaphosphate kinases lead to impaired brain development due to neuronal migration, morphology and synapse formation defects (Rojas et al., 2019; Fu et al., 2017; Fu et al., 2015).

Neural tube defects, caused by a failure of the neural plate to fold, fuse or undergo canalization during neurulation, are highly prevalent congenital abnormalities (reviewed in Greene et al., 2017; Nikolopoulou et al., 2017). Disrupting inositol phosphate metabolism, either through deprivation of dietary inositol or introducing loss-of-function mutations in IP synthesis enzymes, results in or exacerbates cranial neural tube defects (NTDs) (Wilson et al., 2009; Cockroft et al., 1992; Greene and Copp, 1997). Several studies have described additional functions for highly phosphorylated forms of inositol during neural tube closure. Loss of inositol-tetrakisphosphate 1-kinase (ITPK1) and inositol polyphosphate multikinase (IPMK), kinases required for the production of IP5 and its derivatives, result in lethality around the neurulation stage in mice and have been linked to increase in NTD cases in humans (Wilson et al., 2009, Frederik et al., 2005, Guan et al., 2014; Verbsky et al., 2005a).

While numerous genes have been implicated in the development of NTDs in vertebrates, a key category are those that encode for proteins involved in convergent extension (CE). CE is a morphogenetic process marked by the constriction of cell-cell junctions and cell intercalation that act to narrow a tissue along one axis and lengthen it along another (reviewed in Sutherland et al., 2020). Coordination of CE across the neural tube is a prominent driver during the early stages of neurulation, which are dependent upon closure of neuroepithelial folds, and its failure contributes to severe NTDs in vertebrates (Wallingford and Harland, 2002; Goto and Keller, 2002). Components of the conserved Wnt-planar cell polarity (PCP) pathway, such as VANGL1/2 and their orthologues, play important roles in coordinating CE in mice (Lei et al., 2019; Curtin et al., 2003; Murdoch, 2003), *Xenopus* (Wallingford and Harland, 2002; Williams et al., 2014; Butler and Wallingford, 2018) and zebrafish (Ciruna et al., 2006; Reynolds et al., 2010). Besides PCP signaling, junctional contraction during CE are also controlled by transient Ca^{2+} oscillations resulting from the interaction between inositol triphosphate (IP3) and its receptor (Cogram et al., 2004; Politi et al., 2006, Mound et at al., 2017). In support of this, reducing Ca2+ waves through pharmacological or genetic means results in decreased axial elongation and disrupts CE (Wallingford et al., 2001; Westfall et al., 2003). However, the role that more highly phosphorylated forms of inositol play during neural tube development remains poorly understood.

In *C. elegans*, the ventral nerve cord (VNC) assembles in a CE-dependent manner (Shah et al., 2017). The VNC runs along the anterior-posterior (AP) axis of the worm and is comprised of three classes of motor neurons (DD, DA and DB) at hatching. During embryogenesis, neurons

originating from both the left and right sides engage in cell-cell intercalations, including processes facilitated by the formation and resolution of multicellular rosettes, to converge toward the midline. Following this convergence, they are positioned along the AP axis in a predominantly single-file formation. This process involves VANG-1/PCP and SAX-3/Robo-mediated regulation of cell-cell intercalations. Loss of PCP or SAX-3 signaling results in delays in the single file intercalation of neurons, which manifest, in the most severe cases, as a shortened VNC with most neuronal cell bodies displaced anteriorly at hatching (Shah et al., 2017).

In this study, we explore the role of *ippk-1*, the gene encoding the worm orthologue of mammalian inositol-pentakisphosphate 2-kinase (IPPK/IP5K), in VNC assembly (Davis et al., 2022). IPPK is an enzyme in the IP biosynthesis pathway responsible for phosphorylating IP5 to generate IP6 (Verbsky et al., 2002). Our study reveals that the loss of *ippk-1* results in positioning defects of DD neurons within the VNC of newly hatched worms. These defects closely resemble those observed in mutants of *vang-1* and *sax-3*. Disruption of the worm orthologue of IPMK also produces a similar phenotype. Examination of VNC morphogenesis in *ippk-1* mutant embryos uncovered alignment issues as left- and right-derived VNC neurons migrated toward the midline before intercalation. Additionally, we observed defects associated with abnormal CE, such as delayed rosette resolution, a higher occurrence of persistent cell contacts, and reduction in VNC extension by the 1.5-fold stage. DD positioning defects at the first larval stage, a consequence of abnormal VNC development, were rescued by the addition of exogenous IP6. These findings emphasize the importance of IP biosynthesis pathways and polyphosphorylated IPs to central nerve cords that develop through CE-mediated process.

RESULTS

IPPK-1 is required for proper positioning of DD neurons along the VNC.

We have previously shown that disruption of CE-mediated VNC assembly during embryogenesis contributes to the anterior displacement of neurons (Shah et al., 2017). To identify new genes involved in neuron positioning, we performed a genetic screen using the *flp-13p::GFP* (*ynIs37*) DD-specific reporter (unpublished) and identified *zy65*. Whole genome sequencing revealed *zy65* to be mutation in *ippk-1*, the sole *C. elegans* orthologue of IPPK, a kinase in the IP biosynthesis pathway that catalyzes the conversion of IP5 to IP6 (Fig. 1A and B). *ippk-1(zy65)* contains an A to T nucleotide change in the consensus splice acceptor site of exon 6 that is predicted to affect splicing of the *ippk-1* transcript (Fig. 1A).

IPPK-1 was previously shown to be essential for larval growth and in the maintenance of adult germline membrane architecture (Lowry et al., 2015). Our findings indicate an additional role in VNC development. In newly hatched animals, DD neurons display an approximately equidistant spacing along the VNC. In newly hatched *zy65* mutants, DD neurons are located at more anterior positions (Fig. 1C and D). This phenotype is temperature sensitive as there is a significant increase in the penetrance of anteriorly shifted DD neurons when animals are incubated at 25˚C compared to 20˚C (Fig. 1D). We also found that DD position defects are maternally rescued indicating a role for maternally derived IPPK-1 or its product IP6 (Fig. 1D).

We confirmed that the *ippk-1* gene is responsible for the observed DD defects. This was demonstrated through non-complementation with *ippk-1(or1572)*, a temperature-sensitive allele reported in the study by Lowry et al. (data not shown), which also exhibited similar DD

positioning defects (Fig. 1C and D). Due to *or1572* exhibiting sterility or larval arrest at temperatures above 20˚C, we maintained and observed *or1572* at 18˚C to ensure the production of viable larvae. Since IPPK-1 acts in an IP synthesis pathway with several other kinases, we also asked if loss of another kinase in this pathway would also disrupt DD positioning. IPMK phosphorylates both IP3 and IP4 to produce IP5 (Saiardi et al., 1999; Odom et al., 2000). *ipmk-1* is the only *C. elegans* orthologue of IPMK. Unlike *ippk-1*, which is an essential gene, the *ipmk-1(tm2687)* deletion allele, a probable null, is viable (Yang et al., 2021). We found that *tm2687* displayed DD position defects similar to those in *ippk-1* mutants (Fig. 1C and D). As human IPPK has been shown to play additional non-catalytic roles unrelated to IP synthesis (Brehm et al., 2013), these findings indicate that an intact IP kinase cascade is important for proper DD positioning in *C. elegans*.

In addition to defects in the VNC, we also noted that the progeny of *ippk-1(zy65*) worms shifted to 25˚C at L4 also display sterility and epidermal morphology defects similar to those in *ippk-1(or1572)*. Epidermal defects were observed at both embryonic and larval stages. We found that 9.5% (N=116) of post-comma stage embryos and 17.4% (N=135) of larvae displayed epidermal morphology defects characterized by a lumpy appearance, with lumps mostly in the posterior. Notably, loss of upstream components required for the generation of inositol triphosphate (IP3) have been reported to show similar defects in both embryonic and larval stages (Vázquez-Manrique et al., 2008).

<u>*ippk-1* is expressed at low levels.</u>

To determine where *ippk-1* is expressed, we generated two lines in which GFP was inserted at both the N-terminus and C-terminus of the native *ippk-1* gene using the CRISPR/Cas9 homology-directed repair approach described in Dickinson et al. (2015). This approach utilizes a selection cassette (SEC) containing a GFP reporter, followed by a loxP-flanked stop cassette which allows transcriptional read-through past the reporter only upon Cre recombinase-mediated SEC excision. This method has the advantage of allowing an N-terminal insertion to function as a transcriptional reporter before SEC excision and a translational reporter afterwards. Upon examining *ippk-1(zy100[GFP::loxP-stop-loxP::IPPK-1])*, we observed low, potentially ubiquitous GFP transcriptional expression in early larvae, but we could not ascertain any expression in embryos. In the late larval and adult stages, we detected only weak expression in the pharynx and strong expression in the spermatheca (Fig. S1A). With the exception of the spermatheca, we did not observe expression in other areas of the somatic gonad or germline, where we might have expected it, given its role in germline architecture and gonad arm morphology (Lowry et al., 2015). This observation is largely consistent with single-cell transcriptome data, which shows a generally low abundance of *ippk-1* transcripts except in the spermatheca (Taylor et al., 2021; Packer et al., 2019). In both the N-terminal (*zy101*) and C-terminal (*zy102*) GFP translational fusions, we detected expression exclusively in the spermatheca (Fig. S1B).

<u>IPPK-1 acts in concert with VANG-1 and SAX-3 to position DD neurons in the VNC.</u>

We previously demonstrated that the PCP protein VANG-1 and the Robo receptor SAX-3 function in parallel to ensure proper VNC assembly. The simultaneous deletion of both *vang-1* and *sax-3* leads to a synergistic increase in the anterior displacement of VNC neurons, a more pronounced effect than loss of either gene alone (Shah et al., 2017). This more severe anterior shift in double mutants was the result of a more severe disruption in CE movements that shape

the VNC during embryonic development. To investigate genetic interactions between *ippk-1* and these pathways, we examined DD neuron positions in *vang-1* and *sax-3* double mutants. We found that double mutants displayed significantly more severe anterior shifts, at one or more DD neuron positions, compared to *vang-1* and *sax-3* single mutants (Fig. 2A and B). A similar, albeit milder, increase in severity was observed in *vang-1; impk-1* and *sax-3; impk-1* double mutants (Fig. 2A and B). These results are consistent with an *impk-1* and *ippk-1* containing IP pathway acting in concert with *vang-1* and *sax-3* to promote CE during VNC assembly. However, because *ippk-1* is an essential gene and the alleles used in this study are viable and therefore not null alleles, we cannot say conclusively if they act in common or parallel pathways.

<u>*ippk-1* mutants display defective organization of DD and DA neurons at midline contact.</u>

During embryogenesis, DD and DA neuronal precursors, henceforth referred to as neurons, are born on left and right sides and undergo CE-directed migration towards the midline (Shah et al., 2017). To begin to understand how *ippk-1* regulates VNC assembly during this stage, we performed time-lapse microscopy using a *cnd-1p::PH::mCherry* reporter to label the membranes of DD and DA neurons (specifically, DD1-6 and DA1-5). These neurons undergo junctional contractions within a layer of adherent cells as they converge toward the midline (Fig. 3A and B). However, in some *ippk-1* embryos, we found that while movement toward the midline occurred over a similar time interval, these cells appeared to be more compact and less neatly planar in their organization compared to wild-type (WT) embryos (Fig. 3A-D).

To ascertain whether this more compact organization resulted from changes in cell number or fate, we counted the number of *cnd-1p*-labeled neurons at the "lima bean" stage and in L1 animals using terminal cell fate markers. We found a slight but statistically significant reduction (p=0.0131) in the number of *cdn-1p*-labeled cells at "lima bean" stage, with 20 (N=16) in WT and 19 (N=19) in *ippk-1* mutants (Fig. S2A). However, the number of terminally differentiated DD, DA, and DB neurons in L1 animals remained unchanged (Fig. S2B).

In addition to a more compact organization, ippk-1 mutants showed a higher proportion of cnd-1p-labeled neurons from the left and right sides initiating contact at more posterior positions along the midline (Fig. 3C and D). For instance, in WT embryos, only 6.2% (N=32) of neurons approaching the midline made their initial contact in a more posterior region along the midline, whereas in *ippk-1(zy65)* (N=33) and *impk-1(tm2687)* (N=52) mutants, this proportion rose to 42.4% and 25%, respectively (Fig. 3E). They also had an increased number of rosette structures during their initial contact compared to WT organisms (Fig. 3D and F). The proportion of neurons forming rosettes, where five or more cells meet at a common vertex, at the time of midline contact increased from 12.5% in WT (N=32) to 53.6% and 70% in *ippk-1* mutants (N=41) and to 33.3% in *impk-1(tm2687)* mutants (N=54) (Fig. 3F). *vang-1* mutants did not show a significant difference from WT in both the site of initial contact and ectopic rosette formation, suggesting that these phenotypes are specific to disruptions in the IP pathway.

<u>*ippk-1* mutants display defects in convergent extension (CE).</u>

Upon meeting at the midline, DD and DA neurons form multicellular rosettes. The resolution of these rosettes sequentially from anterior to posterior helps drive intercalation at the midline. By the 1.5-fold stage, single-cell intercalations result in a stereotypical pattern of DD and DA neurons aligned in a single file along the lengthening VNC (Shah et al., 2017). Our previous research indicated that the loss of PCP components leads to a slower CE process. This

delay is probably due to the additional time needed for the resolution of rosettes and the intercalation of cells at the midline (Shah et al., 2017). To determine if *ippk-1* regulates rosette dynamics, we performed time-lapse microscopy using *cnd-1p::PH::mCherry* to label DD and DA neurons. In WT, the centrally located rosette resolves on average in less than 4 min after formation. In *ippk-1 zy65* and *or1572* and *impk-1(tm2687)* mutants, the average rosette lifetime increased to 14 min ($p<0.0001$), 17.2 min ($p<0.0001$) and 11.4 min ($p=0.0349$) respectively (Fig. 4A, B and C). As a positive control, we also measured rosette lifetime in *vang-1* mutants and showed that the approximate average time for rosettes to resolve was 12 min ($p=0.0102$) (Fig. 4C). Interestingly, *vang-1(ok1142); ippk-1(zy65)* double mutants (13.2 min) did not show a significant increase in rosette lifetime compared to *zy65* single mutants ($p=0.9985$). This finding may suggest that *ippk-1* and *vang-1* act in a common pathway to regulate rosette dynamics, but because *zy65* is not a null allele and probably retains some IPPK-1 activity, parallel pathways cannot be ruled out.

Single cell intercalation and VNC extension defects were assessed at the 1.5-fold stage just prior to the onset of embryonic twitching using *unc-30p::GFP* (DD) and *cnd-1p::PH::mCherry* reporters (DD and DA). At this stage, most DD and DA neurons have intercalated into a single file with DD1-4 and DA2-5 displaying a stereotypical alternating DD DA pattern (WT in Fig. 4D). We defined an embryo with a cell intercalation defect as one containing at least one abnormal DD-DD cell contact instead of a DD-DA contact. Not surprisingly, given the earlier organization and rosette resolution defects, we found a significant number of single cell intercalation defects in *ippk-1* (36.5%) (N=52, $p=0.007$) and *impk-1* (28.2%) (N=39, $p=0.0114$) mutants compared to WT (7.7%) (N=52) (Fig. 4D and E).

VNC assembly and extension towards the tail appear to be independent of embryo elongation, as a severe disruption of CE during VNC formation does not coincide with a disruption in the transition from the "lima bean" shape to the 3-fold shape (Shah et al., 2017). Therefore, to measure VNC extension at the 1.5-fold stage, we calculated a VNC extension index, defined as the length the VNC extends past the apex of the embryonic fold divided by the overall embryo length. In WT animals, this index is 0.17, whereas it showed a slight but significant decrease to 0.12 in *ippk-1(zy65)* mutants ($p<0.0001$), indicating a shorter posterior extension (Fig. 4F). However, neither *ippk-1(or1572)* nor *impk-1(tm2687)* mutants showed a significant change. Interestingly, within the scored *or1572* embryos, two exhibited an unusually long posterior extension, though the reason for this remains unclear. *vang-1* mutants also showed a small but significant decrease in the extension index to 0.14 ($p=0.0012$). In *vang-1; ippk-1* double mutants, this index decreased even further to 0.09 ($p<0.0001$) and was significantly smaller than *vang-1* and *ippk-1* single mutants alone (each $p<0.0001$) indicating that these proteins normally cooperate to mediate posterior VNC extension (Fig. 4F). Together, defects in rosette resolution, single cell intercalation and posterior VNC extension are consistent with the involvement of *ippk-1* in CE during VNC assembly.

<u>Exogenous IP6 is sufficient to rescue *ippk-1* defects.</u>

In the IP kinase cascade, IPPK-1 phosphorylates IP5 to generate IP6. As a result, we explored whether the introduction of exogenous IP6 could mitigate the phenotypes associated with *ippk-1(zy65)*. To examine this, we performed microinjections of either IP6 (phytic acid) or a control solution into the gonads of *ippk-1(zy65)* worms and subsequently evaluated their

progeny for signs of rescued embryonic midline meeting and larval DD position defects. An examination of IP6 levels in different cells and organisms showed that IP6 concentration ranged from 10µM to 100µM (Szwergold et al., 1987; Freund et al., 1992; Veiga et al., 2006). Consequently, we tested both 10µM to 100µM IP6 concentrations to assess their potential to rescue *ippk-1* mutants.

Injection of IP6 into *ippk-1(zy65)* mutant mothers restored the more anterior positioning of midline contact in *cnd-1*-labeled left and right-side neurons when they met at the midline. *zy65* mutants with midline defects were reduced from 61% (N=31) to 22% (N=34) (p=0.0015) in F1 progeny of mothers injected with 100µM IP6 (Fig. 5A and B). Similarly, exogenous IP6 was able to rescue DD positioning defects in L1 and L2 larvae. In WT, the six DD neurons, visualized with a *flp-13p::GFP* reporter, are typically equidistantly spaced along the VNC, whereas in *zy65* mutants, they are anteriorly displaced. For simplicity, we only assessed the spacing between DD1 and DD2, considering it defective if they were within one cell diameter of each other. In F1 progeny, the occurrence of *zy65* mutants with DD1 DD2 spacing defects decreased significantly from 94% (N=51) to 38% (N=87) and 24% (N=68) when mothers were injected with 10µM or 100µM IP6, respectively (both p<0.0001) (Fig. 5C and D). Injection of IP6 into WT animals did not result in any midline or DD spacing defects in their progeny. As a specificity test, we injected 100µM IP6 into *vang-1* mutant mothers and observed no rescue of DD1 DD2 spacing defects in the F1 progeny (Fig. 5D). This indicates that exogenous IP6 specifically corrects defects associated with IPPK-1 function. These findings show that IP6, the downstream product of IPPK-1, is sufficient to rescue *ippk-1* defects, suggesting that these defects result from an IP6 deficiency.

DISCUSSION

IP molecules, through their regulation of basic cellular processes, play essential roles in early animal embryonic development (Seeds et al., 2015; Frederick et al., 2005; Sarmah et al., 2005; Versky et al., 2005a). The pathway for IP synthesis involves a cascade of inositol kinases that sequentially phosphorylate one of six hydroxyl positions in the inositol ring. It typically commences with PLC and PIP2-derived IP3, ultimately leading to the production of IP6, as well as the higher inositol pyrophosphates IP7 and IP8 (Laha et al., 2021; Majerus, 1992). IPPK is the rate limiting kinase that converts IP5 to IP6, by phosphorylating IP5 at the 2 hydroxyl position of the inositol ring (Verbsky et al., 2005b; Verbsky et al., 2002). In this study, we show that the *C. elegans* orthologue IPPK-1 and its product IP6 are important for proper ventral nerve cord (VNC) morphogenesis.

Loss of *ippk-1* in *C. elegans* leads to embryonic lethality and sterility due to germline membrane defects (Lowry et al., 2015). We found that *ippk-1* mutants also display defects in multiple aspects of the morphogenetic process that leads to the narrowing and lengthening of the layer of adherent DD and DA neurons as they move towards the midline and intercalate to form the VNC. First, they show a more compact and less planar organization of left and right DD and DA progenitors as they converge toward the midline. Second, possibly due to this disorganization, the initial meeting of left and right DD and DA assemblies at the midline often happen at more posterior locations. And third, defects in multicellular rosette resolution and neuron intercalation at the midline. These defects collectively disrupt the normal process of CE,

likely leading to the observed anterior displacement of DD motor neurons in *ippk-1* mutants at hatching.

In metazoans, IP kinases are classified into four groups: IPK, ITPK, IPPK, and PPIP5K, with the IPK group further subdivided into ITP3K, IPMK and IP6K (Laha et al., 2021). Some of these kinases, like ITPK and IPMK are multifunctional and phosphorylate more than one IP ring position (Odom et al., 2000; York et al., 1999). The *C. elegans* genome encodes one orthologue each of ITP3K, IPMK, IPPK and PPIP5K and three orthologues of IP6K. IPMKs catalyze the stepwise phosphorylation of the 6 and 3 hydroxyl positions of IP3 and IP4 respectively to generate IP5. *ipmk-1* mutants display several of the same phenotypic traits displayed by *ippk-1* such as rosette resolution and intercalation defects, and DD displacement defects in newly hatched larvae. This finding, coupled with the rescue of *ippk-1* defects by the exogenous addition of IP6, indicates that *ippk-1* VNC defects are caused by disruption of IP metabolism and not some other factor independent of its catalytic activity.

Surprisingly, the defects in *ipmk-1* were generally milder than those of *ippk-1*, even though the deletion allele we employed was expected to result in a strong loss of function and therefore disrupt IP5 production. In vertebrates, the ability of ITPK, using an alternative PLC-independent pathway, to sequentially phosphorylate hydroxyl positions on IP1 through IP4 to generate IP5, could potentially compensate for the loss of IPMK (Desfougères et al., 2019). However, in contrast to vertebrates, *C. elegans* and several other lower species do not possess a member of the ITPK family (Laha et al., 2021). One possibility, though highly speculative, is that in *C. elegans*, another IP kinase possesses a more adaptable IP binding pocket, enabling it to bind and phosphorylate IP4 molecules. This could explain why losing both *ipmk-1* and *lfe-2* (the ITP3K ortholog) at the same time results in non-viability, even though each gene, when mutated individually, does not affect the organism's viability (Yang et al., 2021).

In a previous study, we found that VANG-1 and PRKL-1, core components of the planar cell polarity pathway (PCP), and SAX-3, a Robo receptor, act in parallel pathways to mediate CE during VNC assembly (Shah et al., 2017). Individual disruption of these pathways result in cell intercalation defects and longer rosette resolution times that may contribute to the anterior displacement of some neurons in the VNC. However, simultaneous loss of both pathways results in a more severe disruption of rosette-mediated CE. For example, in WT, the central rosette that forms at the midline resolves on average in less than 5 minutes, compared to approximately 20 minutes in *sax-3* and *prkl-1* single mutants and greater than 50 minutes in *sax-3; prkl-1* double mutants (Shah et al., 2017). The severe delay in midline intercalation observed in *sax-3; prkl-1* double mutants leads to embryos where, at the time of hatching, nearly all motor neuron cell bodies within the VNC are abnormally positioned towards the anterior half, rather than being evenly dispersed along its entire length.

Compared to PCP and Robo mutants, *ippk-1* mutants display similar defects in rosette resolution, single cell intercalation at the midline and anterior DD displacement. Surprisingly however, the average rosette delay phenotype of *vang-1; ippk-1* double mutants (approximately 12 minutes) was not significantly different than those of single mutants. This suggests that *ippk-1* and *vang-1* may act in a common pathway important for multicellular rosette resolution. A

parallel pathway, however, cannot be excluded as the *ippk-1(zy65)* mutant used in the double is not a null and therefore its role in VNC assembly is not fully understood. Nevertheless, this finding was surprising because, in the same double mutants, the cell bodies of DD neurons, except for DD6, showed more pronounced shifts towards the anterior in larvae compared to those in single mutants. Furthermore, at the 1.5-fold stage, when most DD and DA neurons have intercalated, the length of the developing VNC is mildly but significantly shorter in the double mutant compared to single mutants. These results suggest that *vang-1* and *ippk-1* act in potential parallel pathways, contrasting with a potential shared pathway to mediate rosette resolution. Conceivably, the more severe DD displacement defects observed in *vang-1; ippk-1* double mutants might occur after midline single-cell intercalation, possibly due to the disturbance of another, currently unknown, process. One possibility is a disruption in how DB neurons, positioned ventrally to DD and DA neurons at the 1.5-fold stage, undergo radial intercalation (RI) to insert themselves between DD and DA neurons (Sulston et al., 1983). Notably, convergent extension (CE) and RI represent distinct morphogenetic processes (Sutherland et al., 2020).

The role that IPPK-1 plays in VNC development, a central nerve cord, is interesting in light of evidence that IP metabolism is important for neural tube formation. Several studies have shown that disruptions in IP kinases are associated with neural tube defects. Notably, loss of mammalian ITPK1 leads to embryos that develop NTDs of varying severity, including spina bifida and exencephaly (Wilson et al., 2009). A similar trend can be observed in mutants for the mammalian IPMK/IPK2; although embryos arrest around E9.5, they show multiple morphological abnormalities, which include abnormal folding of the neural tube (Frederick et al., 2005). To date, IPPK gene mutations have not been associated with NTDs, likely due to an essential role for the kinase in embryo development. Loss of mammalian IPPK is lethal, thus preventing a thorough examination of neural tube development (Verbsky et al., 2005a). It should be noted however, that all three genes are expressed in the developing neural tube (Wilson et al., 2009; Frederick et al., 2005; Versky et al., 2005a). This could suggest that they share common mechanisms, similar to what we have shown in our work. Additionally, studies have demonstrated that changes in metabolite concentration may underlie ties between NTDs and IP kinase mutation. ITPK polymorphisms have been associated with increased NTD prevalence and are correlated with lower maternal plasma IP6 concentrations (Guan et al. 2014). Overall lowered maternal myo-inositol concentrations are similarly associated with spina bifida (Groenen et al., 2003). These observations mirror similar trends observed in our maternal rescues of *ippk-1* worms. They also suggest that, given the lack of visible IPPK-1 expression in tissues other than the spermatheca, that low levels of the kinase or metabolite are present in the embryo.

Convergent extension is a predominant driver of neural tube formation across cordate species. In mice, mutations in genes associated with PCP, which are dominant regulators of CE, are closely tied to failed neurulation (Lesko et al., 2021; Williams et al., 2014; Blankenship et al., 2006). This relationship between CE and neural tube development in mice is driven, in part by regulation of junctional dynamics, including the formation and resolution of multicellular rosettes. The failed CE in NTD-bearing mutants is often associated with similar failures in

rosette resolution (Williams et al., 2014). Similarly, CE in other models has been shown to be dependant upon localised junctional dynamics, which require asymmetric distribution of PCP proteins (Shindo et al., 2019; Butler and Wallingford, 2018). IP6 and its derivatives have been previously shown to interact with several membrane and cytoskeletal proteins in *in-vitro* or *in-vivo* models of cell migration and adhesion (Cheng and Andrew, 2015; Fu et al., 2017; Schröterová et al., 2018; Rojas et al., 2019; Bhat et al., 2024). Given the importance of cytoskeleton dynamics in collective cell movements; it is possible that production of these metabolites may help to facilitate membrane dynamics. In line with this, the severe temperature-sensitive *ippk-1* allele *or1752* affects the complex membrane architecture germline which depend on membrane remodeling during oogenesis (Lowry et al., 2015).

Another potential target of *ippk-1*/IP6 is the septin family of cytoskeletal components. Work in Xenopus has shown that septins play important roles in the distribution of actin networks during collective cell behaviors, including convergent extension (Devitt et al., 2024). Septin proteins co-localize and function alongside PCP components, including VANG2 and PRKL2. Recent work from the Burgess lab has shown that an IP6 affinity tag is able to bind with septins proteins in mammal colon cancer models alongside traditional targets found within the nervous system (Yin et al., 2016). This raises the possibility that septins may play a role *ippk-1*-mediated VNC assembly.

Finally, it is possible that production of IP6 could facilitate CE more broadly through the regulation of endocytosis. Several species of inositol phosphates and pyrophosphates are able to bind to components of vesicle transport pathways, including AP-1/2/3, PIP2, synatotagmin-1 and dynamin, where they facilitate both exocytosis and endocytosis (Li et al., 2022, Yang et al., 2012, Høy et al., 2002, Voglmaier et al., 1992). Endocytosis is also broadly required during CE movements, as blocking E-cadherin endocytosis or mutation of dynamin leads to intercalation and tissue extension defects (Levayer et al., 2011; Jarrett et al., 2002). This relationship between endocytosis and CE critically involves intercellular trafficking of PCP pathway components and effectors (Saraswathy et al., 2022; He et al., 2018; Lee et al., 2016; Kida et al., 2007).

In this study, we have explored the involvement of IPPK-1 and its metabolite IP6 in CE during VNC assembly in *C. elegans*. Considering the crucial role CE plays in central nerve cord development, it is important to elucidate the precise mechanism through which IP6 or other inositol phosphates (IPs) regulate this morphogenetic process.

MATERIALS and METHODS

Key Resources

Reagent or resource	Source	Identifier
Chemicals, Peptides, and Recombinant Proteins		
Phytic acid sodium salt hydrate	Sigma-Aldritch	P0109; CAS:14306-25-3
Levamisol hydrochloride	Millipore Sigma	31742; CAS:16595-80-5
Bacterial and Virus Strains		

E. coli: OP50	Caenorhabditis Genetics Center (CGC)	RRID: WB-STRAIN:WBStrain00041969
Experimental Models: Organisms/Strains		
C. elegans: N2 (wild isolate)	Caenorhabditis Genetics Center (CGC)	
C. elegans: ippk-1(zy65) II	This study	N/A
C. elegans: ippk-1(or1572) II	Caenorhabditis Genetics Center (CGC), Lowry et al., 2015.	WB Strain: EU2908; WormBase: WBVar00241916
C. elegans: ippk-1(zy100[GFP::SEC::IPPK-1]) II	This study	N/A
C. elegans: ippk-1(zy102[IPPK-1::GFP]) II	This study	N/A
C. elegans: ynIs37[flp-13p::gfp] III	Caenorhabditis Genetics Center (CGC)	WB Strain: NY2037; WormBase: WBStrain00029158
C. elegans: ipmk-1(tm2687) IV	Dr. Shohei Mitani	N/A
C. elegans: *sax-3(zy5) X*	Antonio Colavita, Shah et al., 2017	N/A
C. elegans: *vang-1(ok1142) X*	Caenorhabditis Genetics Center (CGC)	WB Strain: RB1125; WormBase: WBStrain00031829
C. elegans: *zyIs36(cnd-1::PH::mCherry; myo-2p::mCherry) X*	Antonio Colavita, Shah et al., 2017	N/A
C. elegans: *zyIs40(unc-30p::gfp; cnd-1::PH::mCherry)* Unassigned linkage	This study	N/A
Oligonucleotides		
DNA Oligonucleotides	IDT	See Table S1 for sequences and use.
Software and Algorithms		
Zeiss Zen 3.2	Zeiss	https://www.zeiss.com/microscopy/en/products/software/zeiss-zen.html
Graphpad Prism 10	Graphpad Software	https://www.graphpad.com/scientific-software/prism/
Imaris 10	Oxford Instruments	https://imaris.oxinst.com/

Lead Contact

Further information and requests for resources and reagents should be directed to and will be fulfilled by the lead contact, Antonio Colavita (colavita@uottawa.ca).

Strains and culture conditions

Strains were maintained on NGM plates at 20˚C, except for temperature-sensitive strains, which were maintained at 18ºC. The Bristol N2 strain was used as wild type (WT), along with the following alleles and transgenes: LGII: *ippk-1(zy65), ippk-1(zy101[GFP::3xFLAG::ippk-1]), ippk-1(zy102[ippk-1::GFP::3xFLAG]), ippk-1(or1572), unc-4(syb1658[unc-4::GFP]).* LGIII: *ynIs37[flp-13p::gfp], vab-7(st12267[vab-7::EGFP::3xFLAG]*. LGIV: *ipmk-1(tm2687).* LGX: *sax-3(zy5), vang-1(ok1142), zyIs36[cnd-1p::PH::mCherry myo-2p::mCherry].* Unassigned linkage: *zyIs40[unc-30p::gfp; cnd-1p::PH::mCherry myo-2p::mCherry]*.

Whole genome sequencing and GFP insertion into the endogenous *ippk-1* gene

zy65 was identified in a genetic screen for DD neuron position defects (A Colavita, unpublished) and outcrossed at least 3 times. Single nucleotide variants in the *zy65*-containing strain were identified by whole genome sequencing as described in Noblett et al. (2019).

GFP was inserted into the endogenous *ippk-1* gene at both the N and C-terminus using the CRISPR/Cas9 homology-directed repair (HDR) approach described in Dickinson et al. (2015). Target sites for N-terminal (GAGGATTAATCTGCATTTTC NGG) and C-terminal (AAATGGCCAAATTAAATGCA NGG) insertion were generated using the IDT guide RNA design tool at www.idtdna.com/site/order/designtool/index/CRISPR_SEQUENCE. Guide sequences were inserted into the Cas9–sgRNA plasmid (pDD162, Addgene #47549) using the NEB Q5 Site-Directed Mutagenesis Kit. The HDR plasmid containing *ippk-1* homology arms and the GFP and selection cassette (pDD282, Addgene #66823) was made using Gibson Assembly as described in Dickinson et al. (2015). Sequences were obtained through WormBase (Davis et al., 2022). All primers available on request.

Microscopy and Analysis of Embryonic Phenotypes

For static and timelapse imaging of live embryos, L4 worms were grown at 25˚C, except for *ippk-1(or1572)* which was grown at 18˚C, until gravid. Static imaging were used to quantify the posterior extension of the VNC, presence of persistence-cell contacts and to determine the number of *cnd-1* positive VNC neuroblasts. Embryos were imaged at 63x magnification using using a Zeiss Imager M2, Colibri7 LED source, AxiocamHR camera and Zen V3.2 software.

Tissue measurements were taken with a z-projection of 42 slices with 0.25µm slice width, in a *zyIs36 [cnd-1p::PH::mCherry]* background. Images were processed using a maximum intensity projection prior to analysis. The length of each embryo was measured down the midline starting at the tip of the mouth to the end of the tail. The posterior portion of the VNC was measured starting at the point where it transected the intestinal valve to the end of DD6 (Martin et al., 2016). All images were acquired with an RFP exposure time of 700-900ms at 30% intensity. Images for cell determination counts were taken with the same conditions across the width of the VNC using a 0.5µm slice width. All *cnd-1* positive neurons within the area of the VNC were counted. A representative image of the midline defects was also taken using these settings (Fig. 4C and D) and deconvolved using the constrained iterative algorithm on Zeiss Zen

V3.2. Persistent-cell contact images were taken in a *zyIs40 (unc-30p::GFP cnd-1p::PH::mCherry)* background, with a GFP exposure time of 50ms at 15% intensity and mCherry exposure as above. Images were taken over a z-projection of 1-15 slices with 0.5µm slice width. A persistent cell contact was defined as the failure of WT intercalation between DD1-DD4, in at least two neurons.

Embryos used for time-lapse imaging were collected from plates using a capillary attached to glass pipette, mounted in a 3 µL drop of M9 containing approximately fifty 25 µm diameter polystyrene beads (Polyscience Inc.) and sealed under a coverslip using Vaseline. Fluorescence time-lapse imaging was performed at 63x magnification using the above microscope configuration with a Zeiss SVB1 microscope signal distribution box/*TTL* trigger cable-controlled camera shutter to minimize excitation light induced phototoxicity. Images of "lima bean" stage embryos were acquired at 1.5-minute intervals, for approximately 60-minutes, across a z-projection of 5 to 15 slices with 0.5 µm between slices. 4x4 binning was used to further minimize the required exposure times during timelapse for rosette timing measurements. Timelapse images were taken in a *zyIs36 [cnd-1p::PH::mCherry]* background, with an *mCherry* exposure time of 700ms at 15% intensity. The VNC was scored as having a "meeting defect" if the cells that made contact were approximately in the bottom half of the tissue. Rosette duration was determined as performed in Shah et al. (2017).

Images included in each figure were processed using Zeiss Zen V3.2 and Photoshop. Adjustments were made to the brightness-contrast of each image to standardize representative phenotypes to be easily visible. Deconvolution, using the iterative constrained algorithm on Zen V3.2, was preformed on a representative image of WT and ippk-1(zy65) VNC cells at the midline. 3D reconstructions were made by manually tracing cell outlines in Imaris (Oxford Instruments).

Quantification of neuron number and position in larvae

Eight to ten fourth stage (L4) larval worms were transferred to seeded NGM plates and grown at 25˚C overnight with the exception of *ippk-1(or1572)*, which was grown at 18˚C. Newly hatched first stage larvae (L1) were mounted on 2% agarose pads using 200 µM levamisole (31742, Sigma). DD neuron positions were imaged at 20x magnification and measured as described in Shah et al. (2017). DD, DA and DB neuron counts were scored at 20x magnification using *ynIs37[flp-13p::gfp]* (a gift from Dr. Chris Li, CUNY), *unc-4(syb1658[unc-4::GFP])* and *vab-7(st12267[vab-7::EGFP]* reporters respectively.

Exogenous IP6 rescue

IP6 (phytic acid sodium salt hydrate, P8810, Sigma) was dissolved in ddH_20 to prepare 0.1µM, 10µM and 100µM solutions. These concentrations were chosen, as they cover a range which has been quantified from mammalian and non-mammalian sources (Szwergold et al., 1987; Freund et al., 1992; Veiga et al., 2006). WT, *ippk-1(zy65)* and *vang-1(ok1142)* worms were grown at 18˚C (*zy65*) or 20˚C (WT and *ok1142*) and transferred to 25˚C at 5-6 hours prior to injections. Young adult worms were then injected with IP6 solution into both gonad arms and allowed to recover for 1 hour. Healthy survivors were singled onto seeded NGM plates overnight at 25˚C. Hatched larvae or embryos were mounted on the subsequent morning on 2% agarose pads. L1 and L2 stage worms were scored for the proximity of two or more neurons within a distance of one cell body. Ventral mounted embryos were scored for a shift in the initial

meeting of cells towards the posterior of the embryo (as described above). Progeny from independent worms were pooled for statistical analysis.

Statistics

Larval and embryo measurements were compared across populations with the indicated number of individuals using students' two-tailed t-tests, ANOVA with Tukey's or Dunnett's post hoc test for multiple comparisons and Fisher's exact test for proportions as indicated in figure legends. Zeiss Zen V3.2 was used for image analysis. Graphpad Prism 10 was used for statistical analysis.

ACKNOWLEDGEMENTS

We thank Shohei Mitani for sharing *ipmk-1(tm2687)* and Chris Li for sharing *YnIs37*. Some strains were provided by the Caenorhabditis Genetics Center, which is funded National Institutes of Health Office of Research Infrastructure Programs (P40 OD010440). The authors acknowledge the Cell Biology and Image Acquisition Core (RRID: SCR_021845) funded by the University of Ottawa, Ottawa, Natural Sciences and Engineering Research Council of Canada, and the Canada Foundation for Innovation. Studies presented in this report were supported by research grants from the Canadian Institutes of Health Research (123513) to A. Colavita.

AUTHOR CONTRIBUTIONS

N.N preformed experiments and data analysis. T.R preformed molecular biology procedures. S.F preformed sequence analysis. N.N and A.C wrote the manuscript. A.C supervised the research.

AUTHOR CONTRIBUTIONS

The authors declare no competing interests.

REFERENCES

Ahmed, I., Sbodio, J. I., Harraz, M. M., Tyagi, R., Grima, J. C., Albacarys, L. K., Hubbi, M. E., Xu, R., Kim, S., Paul, B. D., & Snyder, S. H. (2015). Huntington's disease: Neural dysfunction linked to inositol polyphosphate multikinase. *Proceedings of the National Academy of Sciences*, *112*(31), 9751–9756. https://doi.org/10.1073/pnas.1511810112

Bhat, S. A., Malla, A. B., Oddi, V., Sen, J., & Bhandari, R. (2024). Inositol hexakisphosphate kinase 1 is essential for cell junction integrity in the mouse seminiferous epithelium. *Biochimica et Biophysica Acta (BBA)-Molecular Cell Research*, *1871*(1), 119596.

Blankenship, J. T., Backovic, S. T., Sanny, J. S., Weitz, O., & Zallen, J. A. (2006). Multicellular rosette formation links planar cell polarity to tissue morphogenesis. *Developmental cell*, *11*(4), 459-470.

Boitano, S., Dirksen, E. R., & Sanderson, M. J. (1992). Intercellular Propagation of Calcium Waves Mediated by Inositol Trisphosphate. *Science*, *258*(5080), 292–295. https://doi.org/10.1126/science.1411526

Brehm, M. A., Wundenberg, T., Williams, J., Mayr, G. W., & Shears, S. B. (2013). A non-catalytic role for inositol 1,3,4,5,6-pentakisphosphate 2-kinase in the synthesis of ribosomal RNA. *Journal of Cell Science*, *126*(2), 437–444. https://doi.org/10.1242/jcs.110031

Butler, M. T., & Wallingford, J. B. (2018). Spatial and temporal analysis of PCP protein dynamics during neural tube closure. *ELife*, *7*, e36456. https://doi.org/10.7554/eLife.36456

Cheng, Y. L., & Andrew, D. J. (2015). Extracellular Mipp1 activity confers migratory advantage to epithelial cells during collective migration. *Cell reports*, *13*(10), 2174-2188.

Ciruna, B., Jenny, A., Lee, D., Mlodzik, M., & Schier, A. F. (2006). Planar cell polarity signalling couples cell division and morphogenesis during neurulation. *Nature*, *439*(7073), 220–224. https://doi.org/10.1038/nature04375

Cockroft, D. L., Brook, F. A., & Copp, A. J. (1992). Inositol deficiency increases the susceptibility to neural tube defects of genetically predisposed (curly tail) mouse embryos in vitro. *Teratology*, *45*(2), 223–232. https://doi.org/10.1002/tera.1420450216

Cogram, P., Hynes, A., Dunlevy, L. P. E., Greene, N. D. E., & Copp, A. J. (2004). Specific isoforms of protein kinase C are essential for prevention of folate-resistant neural tube defects by inositol. *Human Molecular Genetics*, *13*(1), 7–14. https://doi.org/10.1093/hmg/ddh003

Curtin, J. A., Quint, E., Tsipouri, V., Arkell, R. M., Cattanach, B., Copp, A. J., Henderson, D. J., Spurr, N., Stanier, P., Fisher, E. M., Nolan, P. M., Steel, K. P., Brown, S. D. M., Gray, I. C., & Murdoch, J. N. (2003). Mutation of Celsr1 Disrupts Planar Polarity of Inner Ear Hair Cells and Causes Severe Neural Tube Defects in the Mouse. *Current Biology*, *13*(13), 1129–1133. https://doi.org/10.1016/S0960-9822(03)00374-9

Davis, P., Zarowiecki, M., Arnaboldi, V., Becerra, A., Cain, S., Chan, J., ... & Sternberg, P. W. (2022). WormBase in 2022—data, processes, and tools for analyzing Caenorhabditis elegans. *Genetics*, *220*(4), iyac003.

Desfougères, Y., Wilson, M. S., Laha, D., Miller, G. J., & Saiardi, A. (2019). ITPK1 mediates the lipid-independent synthesis of inositol phosphates controlled by metabolism. *Proceedings of the National Academy of Sciences*, *116*(49), 24551-24561.

Devitt, C. C., Weng, S., Bejar-Padilla, V. D., Alvarado, J., & Wallingford, J. B. (2024). PCP and Septins govern the polarized organization of the actin cytoskeleton during convergent extension. *Current Biology*.

Dickinson, D. J., Pani, A. M., Heppert, J. K., Higgins, C. D., & Goldstein, B. (2015). Streamlined Genome Engineering with a Self-Excising Drug Selection Cassette. *Genetics*, *200*(4), 1035–1049. https://doi.org/10.1534/genetics.115.178335

Efanov, A. M., Zaitsev, S. V., & Berggren, P.-O. (1997). Inositol hexakisphosphate stimulates non-Ca2+-mediated and primes Ca2+-mediated exocytosis of insulin by activation of protein kinase C. *Proceedings of the National Academy of Sciences*, *94*(9), 4435–4439. https://doi.org/10.1073/pnas.94.9.4435

Frederick, J. P., Mattiske, D., Wofford, J. A., Megosh, L. C., Drake, L. Y., Chiou, S.-T., Hogan, B. L. M., & York, J. D. (2005). An essential role for an inositol polyphosphate multikinase, Ipk2, in mouse embryogenesis and second messenger production. *Proceedings of the National Academy of Sciences*, *102*(24), 8454–8459. https://doi.org/10.1073/pnas.0503706102

Freund, W. D., Mayr, G. W., Tietz, C., & Schultz, J. E. (1992). Metabolism of inositol phosphates in the protozoan Paramecium: Characterization of a novel inositol-hexakisphosphate-dephosphorylating enzyme. *European journal of biochemistry*, *207*(1), 359-367.

Fu, C., Xu, J., Li, R. J., Crawford, J. A., Khan, A. B., Ma, T. M., ... & Snyder, S. H. (2015). Inositol hexakisphosphate kinase-3 regulates the morphology and synapse formation of cerebellar purkinje cells via spectrin/adducin. *Journal of Neuroscience*, *35*(31), 11056-11067.

Fu, C., Xu, J., Cheng, W., Rojas, T., Chin, A. C., Snowman, A. M., Harraz, M. M., & Snyder, S. H. (2017). Neuronal migration is mediated by inositol hexakisphosphate kinase 1 via α-actinin and focal adhesion kinase. *Proceedings of the National Academy of Sciences*, *114*(8), 2036–2041. https://doi.org/10.1073/pnas.1700165114

Goto, T., & Keller, R. (2002). The planar cell polarity gene strabismus regulates convergence and extension and neural fold closure in Xenopus. *Developmental Biology*, *247*(1), 165–181. https://doi.org/10.1006/dbio.2002.0673

Greene, N. D. E., & Copp, A. J. (1997). Inositol prevents folate-resistant neural tube defects in the mouse. *Nature Medicine*, *3*(1), 60–66. https://doi.org/10.1038/nm0197-60

Greene, N. D., Leung, K. Y., & Copp, A. J. (2017). Inositol, neural tube closure and the prevention of neural tube defects. *Birth defects research*, *109*(2), 68-80.

Groenen, P. M., Peer, P. G., Wevers, R. A., Swinkels, D. W., Franke, B., Mariman, E. C., & Steegers-Theunissen, R. P. (2003). Maternal myo-inositol, glucose, and zinc status is associated with the risk of offspring with spina bifida. *American Journal of Obstetrics and Gynecology*, *189*(6), 1713–1719. https://doi.org/10.1016/S0002-9378(03)00807-X

Guan, Z., Wang, J., Guo, J., Wang, F., Wang, X., Li, G., Xie, Q., Han, X., Niu, B., & Zhang, T. (2014). The Maternal ITPK1 Gene Polymorphism Is Associated with Neural Tube Defects in a High-Risk Chinese Population. *PLOS ONE*, *9*(1), e86145. https://doi.org/10.1371/journal.pone.0086145

He, C. W., Liao, C. P., Chen, C. K., Teulière, J., Chen, C. H., & Pan, C. L. (2018). The polarity protein VANG-1 antagonizes Wnt signaling by facilitating Frizzled endocytosis. *Development*, *145*(24), dev168666.

Høy, M., Efanov, A. M., Bertorello, A. M., Zaitsev, S. V., Olsen, H. L., Bokvist, K., ... & Gromada, J. (2002). Inositol hexakisphosphate promotes dynamin I-mediated endocytosis. *Proceedings of the National Academy of Sciences*, *99*(10), 6773-6777.

Jadav, R. S., Kumar, D., Buwa, N., Ganguli, S., Thampatty, S. R., Balasubramanian, N., & Bhandari, R. (2016). Deletion of inositol hexakisphosphate kinase 1 (IP6K1) reduces cell

migration and invasion, conferring protection from aerodigestive tract carcinoma in mice. *Cellular Signalling*, *28*(8), 1124–1136. https://doi.org/10.1016/j.cellsig.2016.04.011

Jarrett, O., Stow, J. L., & Key, B. (2002). Dynamin-dependent endocytosis is necessary for convergent-extension movements in Xenopus animal cap explants. *The International journal of developmental biology*, *46*(4), 467-473.

Kida, Y. S., Sato, T., Miyasaka, K. Y., Suto, A., & Ogura, T. (2007). Daam1 regulates the endocytosis of EphB during the convergent extension of the zebrafish notochord. *Proceedings of the National Academy of Sciences*, *104*(16), 6708-6713.

Laha, D., Portela-Torres, P., Desfougères, Y., & Saiardi, A. (2021). Inositol phosphate kinases in the eukaryote landscape. *Advances in biological regulation*, *79*, 100782. Lei, Y., Kim, S.-E., Chen, Z., Cao, X., Zhu, H., Yang, W., Shaw, G. M., Zheng, Y., Zhang, T., Wang, H.-Y., & Finnell, R. H. (2019). Variants identified in PTK7 associated with neural tube defects. *Molecular Genetics & Genomic Medicine*, *7*(4), e00584. https://doi.org/10.1002/mgg3.584

Lee, H., Lee, S. J., Kim, G. H., Yeo, I., & Han, J. K. (2016). PLD1 regulates Xenopus convergent extension movements by mediating Frizzled7 endocytosis for Wnt/PCP signal activation. *Developmental Biology*, *411*(1), 38-49.

Lei, Y., Kim, S.-E., Chen, Z., Cao, X., Zhu, H., Yang, W., Shaw, G. M., Zheng, Y., Zhang, T., Wang, H.-Y., & Finnell, R. H. (2019). Variants identified in PTK7 associated with neural tube defects. *Molecular Genetics & Genomic Medicine*, *7*(4), e00584. https://doi.org/10.1002/mgg3.584

Lesko, A. C., Keller, R., Chen, P., & Sutherland, A. (2021). Scribble mutation disrupts convergent extension and apical constriction during mammalian neural tube closure. *Developmental Biology*, *478*, 59–75. https://doi.org/10.1016/j.ydbio.2021.05.013

Levayer, R., Pelissier-Monier, A., & Lecuit, T. (2011). Spatial regulation of Dia and Myosin-II by RhoGEF2 controls initiation of E-cadherin endocytosis during epithelial morphogenesis. *Nature cell biology*, *13*(5), 529-540.

Li, H., Datunashvili, M., Reyes, R. C., & Voglmaier, S. M. (2022). Inositol hexakisphosphate kinases differentially regulate trafficking of vesicular glutamate transporters 1 and 2. *Frontiers in Cellular Neuroscience*, *16*, 926794.

Loss, O., Wu, C. T., Riccio, A., & Saiardi, A. (2013). Modulation of inositol polyphosphate levels regulates neuronal differentiation. *Molecular Biology of the Cell*, *24*(18), 2981–2989. https://doi.org/10.1091/mbc.e13-04-0198

Lowry, J., Yochem, J., Chuang, C.-H., Sugioka, K., Connolly, A. A., & Bowerman, B. (2015). High-Throughput Cloning of Temperature-Sensitive Caenorhabditis elegans Mutants with Adult Syncytial Germline Membrane Architecture Defects. *G3 Genes|Genomes|Genetics*, *5*(11), 2241–2255. https://doi.org/10.1534/g3.115.021451

Majerus, P. W. (1992). Inositol phosphate biochemistry. *Annual review of biochemistry*, *61*(1), 225-250.

Martin, E., Rocheleau-Leclair, O., & Jenna, S. (2016). Novel metrics to characterize embryonic elongation of the nematode Caenorhabditis elegans. *JoVE (Journal of Visualized Experiments)*, (109), e53712.

Mound, A., Vautrin-Glabik, A., Foulon, A., Botia, B., Hague, F., Parys, J. B., Ouadid-Ahidouch, H., & Rodat-Despoix, L. (2017). Downregulation of type 3 inositol (1,4,5)-trisphosphate receptor decreases breast cancer cell migration through an oscillatory Ca2+ signal. *Oncotarget*, *8*(42), 72324–72341. https://doi.org/10.18632/oncotarget.20327

Murdoch, J. N., Henderson, D. J., Doudney, K., Gaston-Massuet, C., Phillips, H. M., Paternotte, C., Arkell, R., Stanier, P., & Copp, A. J. (2003). Disruption of scribble (Scrb1) causes severe neural tube defects in the circletail mouse. *Human Molecular Genetics*, *12*(2), 87–98. https://doi.org/10.1093/hmg/ddg014

Nikolopoulou, E., Galea, G. L., Rolo, A., Greene, N. D. E., & Copp, A. J. (2017). Neural tube closure: Cellular, molecular and biomechanical mechanisms. *Development (Cambridge, England)*, *144*(4), 552–566. https://doi.org/10.1242/dev.145904

Noblett, N., Wu, Z., Ding, Z. H., Park, S., Roenspies, T., Flibotte, S., ... & Colavita, A. (2019). DIP-2 suppresses ectopic neurite sprouting and axonal regeneration in mature neurons. *Journal of Cell Biology*, *218*(1), 125-133.

Odom, A. R., Stahlberg, A., Wente, S. R., & York, J. D. (2000). A Role for Nuclear Inositol 1,4,5-Trisphosphate Kinase in Transcriptional Control. *Science*, *287*(5460), 2026–2029. https://doi.org/10.1126/science.287.5460.2026

Packer, J. S., Zhu, Q., Huynh, C., Sivaramakrishnan, P., Preston, E., Dueck, H., Stefanik, D., Tan, K., Trapnell, C., Kim, J., Waterston, R. H., & Murray, J. I. (2019). A lineage-resolved molecular atlas of C. elegans embryogenesis at single-cell resolution. *Science*, *365*(6459), eaax1971. https://doi.org/10.1126/science.aax1971

Park, J., Longo, F., Park, S. J., Lee, S., Bae, M., Tyagi, R., Han, J.-H., Kim, S., Santini, E., Klann, E., & Snyder, S. H. (2019a). Inositol polyphosphate multikinase mediates extinction of fear memory. *Proceedings of the National Academy of Sciences*, *116*(7), 2707–2712. https://doi.org/10.1073/pnas.1812771116

Park, J., Park, S. J., & Kim, S. (2019b). Inositol polyphosphate multikinase deficiency leads to aberrant induction of synaptotagmin-2 in the forebrain. *Molecular Brain*, *12*(1), 58. https://doi.org/10.1186/s13041-019-0480-1

Politi, A., Gaspers, L. D., Thomas, A. P., & Höfer, T. (2006). Models of IP3 and Ca2+ Oscillations: Frequency Encoding and Identification of Underlying Feedbacks. *Biophysical Journal*, *90*(9), 3120–3133. https://doi.org/10.1529/biophysj.105.072249

Rao, F., Xu, J., Fu, C., Cha, J. Y., Gadalla, M. M., Xu, R., Barrow, J. C., & Snyder, S. H. (2015). Inositol pyrophosphates promote tumor growth and metastasis by antagonizing liver kinase B1. *Proceedings of the National Academy of Sciences*, *112*(6), 1773–1778. https://doi.org/10.1073/pnas.1424642112

Reynolds, A., McDearmid, J. R., Lachance, S., De Marco, P., Merello, E., Capra, V., ... & Kibar, Z. (2010). VANGL1 rare variants associated with neural tube defects affect convergent extension in zebrafish. *Mechanisms of development*, *127*(7-8), 385-392.

Rojas, T., Cheng, W., Gao, Z., Liu, X., Wang, Y., Malla, A. P., Chin, A. C., Romer, L. H., Snyder, S. H., & Fu, C. (2019). Inositol hexakisphosphate kinase 3 promotes focal adhesion turnover via interactions with dynein intermediate chain 2. *Proceedings of the National Academy of Sciences*, *116*(8), 3278–3287. https://doi.org/10.1073/pnas.1817001116

Saiardi, A., Erdjument-Bromage, H., Snowman, A. M., Tempst, P., & Snyder, S. H. (1999). Synthesis of diphosphoinositol pentakisphosphate by a newly identified family of higher inositol polyphosphate kinases. *Current Biology*, *9*(22), 1323–1326. https://doi.org/10.1016/S0960-9822(00)80055-X

Saraswathy, V. M., Kurup, A. J., Sharma, P., Polès, S., Poulain, M., & Fürthauer, M. (2022). The E3 ubiquitin ligase mindbomb1 controls planar cell polarity-dependent convergent extension movements during zebrafish gastrulation. *Elife*, *11*, e71928.

Sarmah, B., Latimer, A. J., Appel, B., & Wente, S. R. (2005). Inositol Polyphosphates Regulate Zebrafish Left-Right Asymmetry. *Developmental Cell*, *9*(1), 133–145. https://doi.org/10.1016/j.devcel.2005.05.002

Schröterová, L., Ježková, A., Rudolf, E., Caltová, K., Králová, V., & Hanušová, V. (2018). Inositol hexaphosphate limits the migration and the invasiveness of colorectal carcinoma cells in vitro. *International Journal of Oncology*, *53*(4), 1625-1632.

Seeds, A. M., Tsui, M. M., Sunu, C., Spana, E. P., & York, J. D. (2015). Inositol phosphate kinase 2 is required for imaginal disc development in Drosophila. *Proceedings of the National Academy of Sciences*, *112*(51), 15660–15665. https://doi.org/10.1073/pnas.1514684112

Shah, P. K., Tanner, M. R., Kovacevic, I., Rankin, A., Marshall, T. E., Noblett, N., Tran, N. N., Roenspies, T., Hung, J., Chen, Z., Slatculescu, C., Perkins, T. J., Bao, Z., & Colavita, A. (2017). PCP and SAX-3/Robo Pathways Cooperate to Regulate Convergent Extension-Based Nerve Cord Assembly in C. elegans. *Developmental Cell*, *41*(2), 195-203.e3. https://doi.org/10.1016/j.devcel.2017.03.024

Shindo, A., Inoue, Y., Kinoshita, M., & Wallingford, J. B. (2019). PCP-dependent transcellular regulation of actomyosin oscillation facilitates convergent extension of vertebrate tissue. *Developmental biology*, *446*(2), 159-167.

Sulston, J. E., Schierenberg, E., White, J. G., & Thomson, J. N. (1983). The embryonic cell lineage of the nematode Caenorhabditis elegans. *Developmental biology*, *100*(1), 64-119.

Sutherland, A., Keller, R., & Lesko, A. (2020). Convergent extension in mammalian morphogenesis. In *Seminars in cell & developmental biology* (Vol. 100, pp. 199-211). Academic Press.

Szwergold, B. S., Graham, R. A., & Brown, T. R. (1987). Observation of inositol pentakis-and hexakis-phosphates in mammalian tissues by 31P NMR. *Biochemical and biophysical research communications*, *149*(3), 874-881.

Taylor, S. R., Santpere, G., Weinreb, A., Barrett, A., Reilly, M. B., Xu, C., ... & Miller, D. M. (2021). Molecular topography of an entire nervous system. *Cell*, *184*(16), 4329-4347.

Ucuncu, E., Rajamani, K., Wilson, M. S. C., Medina-Cano, D., Altin, N., David, P., Barcia, G., Lefort, N., Banal, C., Vasilache-Dangles, M.-T., Pitelet, G., Lorino, E., Rabasse, N., Bieth, E., Zaki, M. S., Topcu, M., Sonmez, F. M., Musaev, D., Stanley, V., … Cantagrel, V. (2020). MINPP1 prevents intracellular accumulation of the chelator inositol hexakisphosphate and is mutated in Pontocerebellar Hypoplasia. *Nature Communications*, *11*(1), 6087. https://doi.org/10.1038/s41467-020-19919-y

Vázquez-Manrique, R. P., Nagy, A. I., Legg, J. C., Bales, O. A. M., Ly, S., & Baylis, H. A. (2008). Phospholipase C-ε Regulates Epidermal Morphogenesis in Caenorhabditis elegans. *PLOS Genetics*, *4*(3), e1000043. https://doi.org/10.1371/journal.pgen.1000043

Veiga, N., Torres, J., Domínguez, S., Mederos, A., Irvine, R. F., Díaz, A., & Kremer, C. (2006). The behaviour of myo-inositol hexakisphosphate in the presence of magnesium (II) and calcium (II): protein-free soluble InsP6 is limited to 49 μM under cytosolic/nuclear conditions. *Journal of inorganic biochemistry*, *100*(11), 1800-1810.

Verbsky, J. W., Wilson, M. P., Kisseleva, M. V., Majerus, P. W., & Wente, S. R. (2002). The Synthesis of Inositol Hexakisphosphate: CHARACTERIZATION OF HUMAN INOSITOL 1,3,4,5,6-PENTAKISPHOSPHATE 2-KINASE *. *Journal of Biological Chemistry*, *277*(35), 31857–31862. https://doi.org/10.1074/jbc.M205682200

Verbsky, J., Lavine, K., & Majerus, P. W. (2005a). Disruption of the mouse inositol 1,3,4,5,6-pentakisphosphate 2-kinase gene, associated lethality, and tissue distribution of 2-kinase expression. *Proceedings of the National Academy of Sciences*, *102*(24), 8448–8453. https://doi.org/10.1073/pnas.0503656102

Verbsky, J. W., Chang, S. C., Wilson, M. P., Mochizuki, Y., & Majerus, P. W. (2005b). The pathway for the production of inositol hexakisphosphate in human cells. *Journal of Biological Chemistry*, *280*(3), 1911-1920.

Voglmaier, S. M., Keen, J. H., Murphy, J. E., Ferris, C. D., Prestwich, G. D., Snyder, S. H., & Theibert, A. B. (1992). Inositol hexakisphosphate receptor identified as the clathrin assembly protein AP-2. *Biochemical and biophysical research communications*, *187*(1), 158-163.

Wallingford, J. B., Ewald, A. J., Harland, R. M., & Fraser, S. E. (2001). Calcium signaling during convergent extension in Xenopus. *Current Biology*, *11*(9), 652–661. https://doi.org/10.1016/S0960-9822(01)00201-9

Wallingford, J. B., & Harland, R. M. (2002). Neural tube closure requires Dishevelled-dependent convergent extension of the midline. *Development*, *129*(24), 5815–5825. https://doi.org/10.1242/dev.00123

Westfall, T. A., Brimeyer, R., Twedt, J., Gladon, J., Olberding, A., Furutani-Seiki, M., & Slusarski, D. C. (2003). Wnt-5/pipetail functions in vertebrate axis formation as a negative regulator of Wnt/β-catenin activity. *Journal of Cell Biology*, *162*(5), 889–898. https://doi.org/10.1083/jcb.200303107

Williams, M., Yen, W., Lu, X., & Sutherland, A. (2014). Distinct Apical and Basolateral Mechanisms Drive Planar Cell Polarity-Dependent Convergent Extension of the Mouse Neural Plate. *Developmental Cell*, *29*(1), 34–46. https://doi.org/10.1016/j.devcel.2014.02.007

Wilson, M. P., Hugge, C., Bielinska, M., Nicholas, P., Majerus, P. W., & Wilson, D. B. (2009). Neural tube defects in mice with reduced levels of inositol 1,3,4-trisphosphate 5/6-kinase. *Proceedings of the National Academy of Sciences*, *106*(24), 9831–9835. https://doi.org/10.1073/pnas.0904172106

Yang, S.-N., Yu, J., Mayr, G. W., Hofmann, F., Larsson, O., & Berggren, P.-O. (2001). Inositol hexakisphosphate increases L-type Ca2+ channel activity by stimulation of adenylyl cyclase. *The FASEB Journal*, *15*(10), 1753–1763. https://doi.org/10.1096/fj.00-0799com

Yang, S. N., Shi, Y., Yang, G., Li, Y., Yu, L., Shin, O. H., ... & Berggren, P. O. (2012). Inositol hexakisphosphate suppresses excitatory neurotransmission via synaptotagmin-1 C2B domain in the hippocampal neuron. *Proceedings of the National Academy of Sciences*, *109*(30), 12183-12188.

Yang, Z.-L., Chen, J.-N., Lu, Y.-Y., Lu, M., Wan, Q.-L., Wu, G.-S., & Luo, H.-R. (2021). Inositol polyphosphate multikinase IPMK-1 regulates development through IP3/calcium signaling in Caenorhabditis elegans. *Cell Calcium*, *93*, 102327. https://doi.org/10.1016/j.ceca.2020.102327

Yin, M. X., Catimel, B., Gregory, M., Condron, M., Kapp, E., Holmes, A. B., & Burgess, A. W. (2016). Synthesis of an inositol hexakisphosphate (IP6) affinity probe to study the interactome from a colon cancer cell line. *Integrative Biology*, *8*(3), 309-318.

York, J. D., Odom, A. R., Murphy, R., Ives, E. B., & Wente, S. R. (1999). A phospholipase C-dependent inositol polyphosphate kinase pathway required for efficient messenger RNA export. *Science*, *285*(5424), 96-100.

Figure Legends

Figure 1. *ippk-1* mutants display DD neuron spacing defects. (A) Diagram of the *ippk-1* genomic region labeled with allele and GFP fusions used in this study. (B) Schematic showing kinase cascade involved in phosphorylating IP4 and IP5 to produce IP6. (C) Representative images of DD positions in WT, *ippk-1* and *ipmk-1* mutants, visualised using the DD-specific *flp-13p::GFP* reporter. Arrowheads mark DD neurons. Scale bar = 20µm. (D) Quantification of DD2–4 positions relative to DD1 in L1 stage WT and mutant worms. Neurons (colour coded as indicated along top) are plotted along the AP axis, where DD1 and anus mark the 0% and 100% positions respectively. Means and 95% confidence intervals are indicated for each DD2-6 neuron and animals scored (N) indicated on the right. Significance was determined using a one-way ANOVA with Dunnett's post-hoc test against the corresponding WT neuron, except for strains scored at 20ºC, where a two-tailed t-test was used. *p<0.05, **p<0.01, ***p<0.001.

Figure 2. DD position defects are more severe in *vang-1; ippk-1* and *sax-3; ippk-1* double mutants compared to single mutants. (A) Representative images and (B) quantification of DD neuron position defects in *vang-1* and *sax-3* single or combined with *ippk-1* and *ipmk-1* mutants.

Scale bar is 20μm. Means, 95% confidence intervals and plot format as in Fig. 1D. Significance was determined using one-way ANOVA with Tukey's post-hoc test against the corresponding neuron of the genotype shown on the rightmost column. Single mutants were compared against WT. Double mutants were compared to *vang-1(ok1142)* or *sax-3(zy5)* single mutants. *p<0.05, **p<0.01, ***p<0.001.

Figure 3. *ippk-1* mutants display defective organization of DD and DA neuroblasts prior to and during midline contact. (A-B) Time-lapse fluorescence images showing the migration of *cnd-1p::PH::mCherry*-labeled neurons, including a subset of DD and DA neurons, from left and right sides toward the midline in (A) WT and (B) *ippk-1(zy65)* embryos. Arrows indicate midline contact. (C-D) Deconvolved Z-stack images of a representative WT (C) and *zy65* (D) embryo at midline contact, revealing a more compact and less planar arrangement of neurons in *zy65* embryos. The magenta outline indicates an ectopic rosette. Arrows indicate midline contact. (E) Diagram and quantification of the proportion of WT and mutant embryos displaying initial midline contact in more posterior positions. Green dotted lines indicates approximate divisions for each VNC. (F) Quantification of the proportion of WT and mutant embryos displaying ectopic rosettes at initial midline contact. For E and F, error bars indicate SEP. Significance compared to WT was determined using Fisher's exact test. *p<0.05, **p<0.01, ***p<0.001. Scale bars = 10μm.

Figure 4. *ippk-1(zy65)* mutants display defects in cell-cell intercalations and central rosette timing. (A-B) Timelapse of the formation and resolution of a central VNC rosette in (A) WT and (B) *ippk-1(zy65)* embryos with a *zyIs36[cnd-1::PH::RFP; myo-2p::mCherry]* background. The engaged rosettes are indicated by the magenta line. Schematic of the rosette lifetime is shown below the timelapse. Green indicates expanding junctions. (C) Quantification of central rosette duration. Tails indicate min and max. Statistics: ANOVA with Tukey's post-hoc test. Asterisk indicate significance compared to WT. (D) Deconvolved images of the VNC in WT and mutant embryo at 1.5 fold stage in a *zyIs40[unc-30p::gfp;cnd-1::PH::RFP]* background. The magenta box indicates the approximate area of the VNC in the middle panels. Schematics of each embryo highlight the position of cells, with green indicating DD neuron positions. (E) Quantification of persistent cell contacts within WT and mutant embryos. Error bars indicate SEP. Statistics: Fisher's exact test. (F) Left: Quantification of posterior VNC extension in WT and mutant embryos, relative to total embryo length. Right: Panels show an image and schematic of a WT embryo with magenta lines indicating the lengths measured. Tails indicate min and max. Statistics: ANOVA with Tukey's post-hoc test. *p<0.05, **p<0.01, ***p<0.001. Scale bars = 10μm.

Figure 5. Exogenous IP6 is sufficient to rescue *ippk-1(zy65)* VNC defects. (A) Images of *ippk-1(zy65)* embryos injected with either a control or IP6. Scale bar = 10μm. (B) Quantification of the proportion of WT and mutant embryos displaying initial midline contact in more posterior positions. (C) Images of *ippk-1(zy65)* larvae injected with either a control or IP6. Arrowheads mark DD neurons. Scale bar = 20μm. (D) Quantification of the proportion of WT and mutant larvae displaying a DD1 DD2 spacing defect. For both B and D, error bars indicate SEP. Significance compared to WT was determined using Fisher's exact test. **p<0.01, ***p<0.001.

Supplemental Figure 1. Endogenous *ippk-1* expression. Endogenous *ippk-1* expression in adults from GFP (A) transcriptional (*zy100[GFP::loxPstoploxP::IPPK-1)* and (B) translational

(zy102[IPPK-1::GFP]) fusions showing expression in spermatheca (white arrows). Corresponding Nomarski image above fluorescence image. Scale bar = 20µm.

Supplemental Figure 2. *ippk-1(zy65)* does not cause defects in terminal VNC cell fates.

(A) Quantification of the number of midbody cells expressing *cnd-1p::PH::RFP* in WT and *ippk-1(zy65)*. (B) Quantification of the number of VNC neurons expressing a *flip-13p::GFP* (DD), *unc-4p::GFP* (DA) or *vab-7p::GFP* (DB) reporter in WT and *ippk-1(zy65)* L1 larvae. Statistics: Mann-Whitney U test. *p<0.05, **p<0.01, ***p<0.001.

Supplemental Table 1: Oligos used in this study.

Oligo #	DNA Oligos Sequence (5' – 3')	Source	Use
N1	AAATGGCCAAATTAAATGCAGTTTTAGAG CTAGAAATAGCAAGT	IDT	SGRNA for C-terminal insertion of GFP
N2	CAAGACATCTCGCAATAGG	IDT	SGRNA universal reverse primer
N3	ACGTTGTAAAACGACGGCCAGTCGCCGGC AGGTCATATTTCGGCGGATGT	IDT	5' Repair template for C-terminal insertion of GFP
N4	CATCGATGCTCCTGAGGCTCCCGATGCTCC AATGCACGGCTTAAAATTTCGC	IDT	5' Repair template for C-terminal insertion of GFP
N5	CGTGATTACAAGGATGACGATGACAAGAG ATAATTTGGCCATTTTTTGCATCAA	IDT	3' Repair template for C-terminal insertion of GFP
N6	GGAAACAGCTATGACCATGTTATCGATTTC AGGAAATTGGAAATGTACGTGG	IDT	3' Repair template for C-terminal insertion of GFP
N7	GAGGATTAATCTGCATTTTCGTTTTAGAGC TAGAAATAGCAAGT	IDT	SGRNA for N-terminal insertion of GFP
N8	ACGTTGTAAAACGACGGCCAGTCGCCGGC AGTTTCCGCAGAATCCCCATC	IDT	5' Repair template for N -terminal insertion of GFP
N9	TCCAGTGAACAATTCTTCTCCTTTACTCAT TTTCGGGTGGTTTTGGTGAG	IDT	5' Repair template for N -terminal insertion of GFP
N10	CGTGATTACAAGGATGACGATGACAAGAG AATGCAGATTAATCCTCCTGCA	IDT	3' Repair template for N -terminal insertion of GFP
N11	TCACACAGGAAACAGCTATGACCATGTTA TCCACGAGGGGCATTTCAAAT	IDT	3' Repair template for N-terminal insertion of GFP
N12	CATTTTGCTCTTGGAATAACGCA	IDT	Sequence *ippk-1(zy65)*

N13	TTTGTCCAGGAGGCTTGTCT	IDT	Sequence *ippk-1(zy65)*
N14	GTTGACGTACATCAGCTCGC	IDT	Sequence *ippk-1(or1572)*
N15	TGGACACACAGAATAAGCGC	IDT	Sequence *ippk-1(or1572)*
N16	TCTCCACCCAAAACTCAGGA	IDT	Genotype *ipmk-1(tm2687)*
N17	CACCTCTGAACCTATACCGCT	IDT	Genotype ipmk-1(tm2687)
N18	ACCCTGCAATATCCGGTTCA	IDT	Genotype *ipmk-1(tm2687)*
N19	TTCACCTTGACAACGCCAGA	IDT	Genotype *vang-1(ok1142)*
N20	GGCATGATGACTAGCCCACAA	IDT	Genotype *vang-1(ok1142)*
N21	TGTGACAGGGAAAAGTGGAC	IDT	Genotype *vang-1(ok1142)*
N22	TTCCTGTGATTGTCATTGTTGC	IDT	Genotype *sax-3(zy5)*
N23	TCGATCGAGATCGTCTTCCA	IDT	Genotype *sax-3(zy5)*

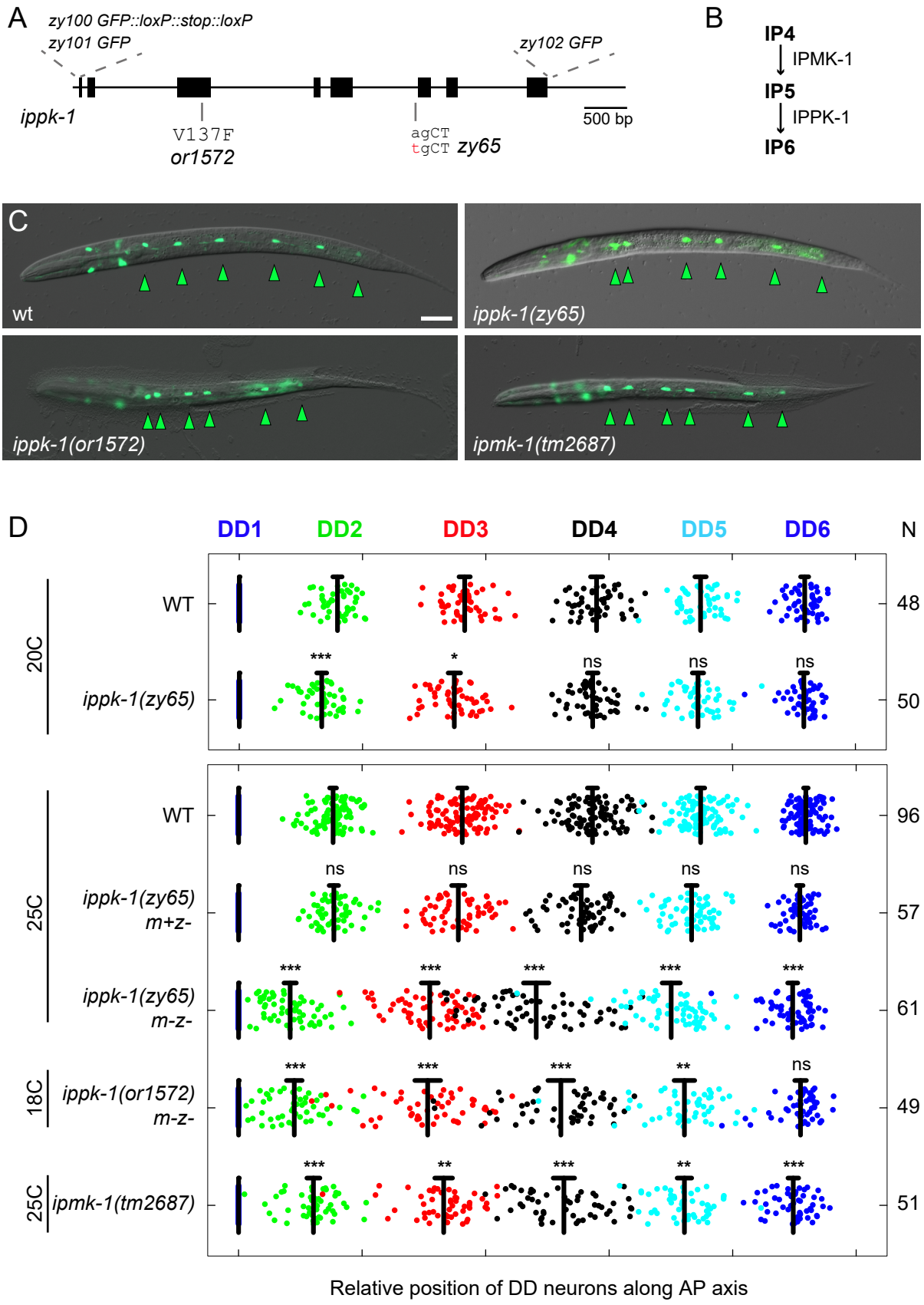
A
zy100 GFP::loxP::stop::loxP
zy101 GFP
zy102 GFP
ippk-1
V137F
or1572
agCT
tgCT
zy65
500 bp
B
IP4
IPMK-1
IP5
IPPK-1
IP6
C
wt
ippk-1(zy65)
ippk-1(or1572)
ipmk-1(tm2687)
D
DD1
DD2
DD3
DD4
DD5
DD6
N
20C
WT
48
ippk-1(zy65)
50
25C
WT
96
ippk-1(zy65) m+z-
57
ippk-1(zy65) m-z-
61
18C
ippk-1(or1572) m-z-
49
25C
ipmk-1(tm2687)
51
Relative position of DD neurons along AP axis

FIG 1

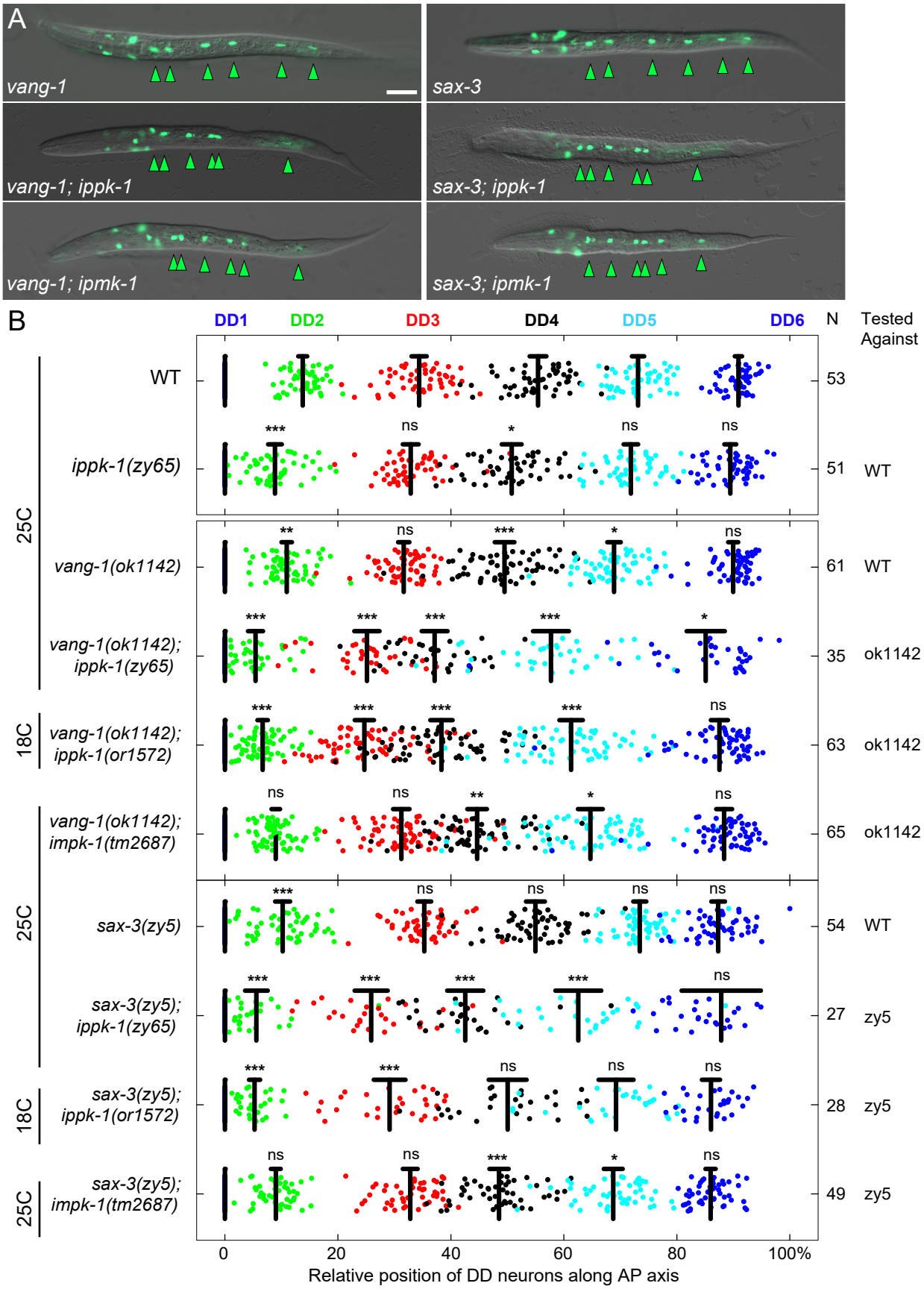
A
vang-1
sax-3
vang-1; ippk-1
sax-3; ippk-1
vang-1; ipmk-1
sax-3; ipmk-1
B
DD1
DD2
DD3
DD4
DD5
DD6
N
Tested Against
WT
53
ippk-1(zy65)
51
WT
vang-1(ok1142)
61
WT
vang-1(ok1142); ippk-1(zy65)
35
ok1142
vang-1(ok1142); ippk-1(or1572)
63
ok1142
vang-1(ok1142); impk-1(tm2687)
65
ok1142
sax-3(zy5)
54
WT
sax-3(zy5); ippk-1(zy65)
27
zy5
sax-3(zy5); ippk-1(or1572)
28
zy5
sax-3(zy5); impk-1(tm2687)
49
zy5
25C
18C
0
20
40
60
80
100%
Relative position of DD neurons along AP axis

FIG 2

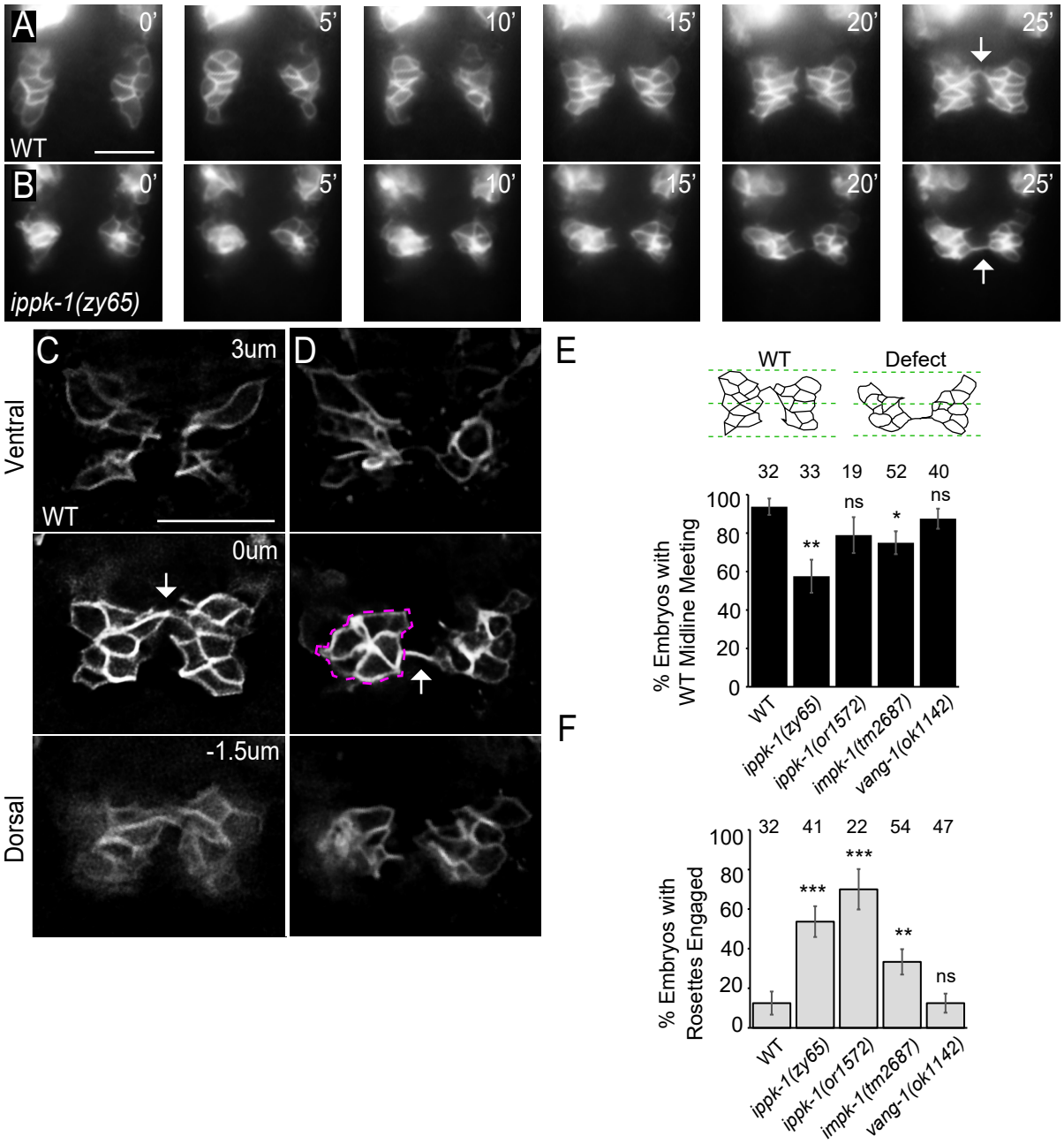
A
0'
5'
10'
15'
20'
25'
WT
B
ippk-1(zy65)
C
3um
0um
-1.5um
Ventral
Dorsal
D
E
WT
Defect
F
% Embryos with WT Midline Meeting
32 33 19 52 40
ns
**
*
ns
WT
ippk-1(zy65)
ippk-1(or1572)
impk-1(tm2687)
vang-1(ok1142)
% Embryos with Rosettes Engaged
32 41 22 54 47
***
***
**
ns

FIG 3

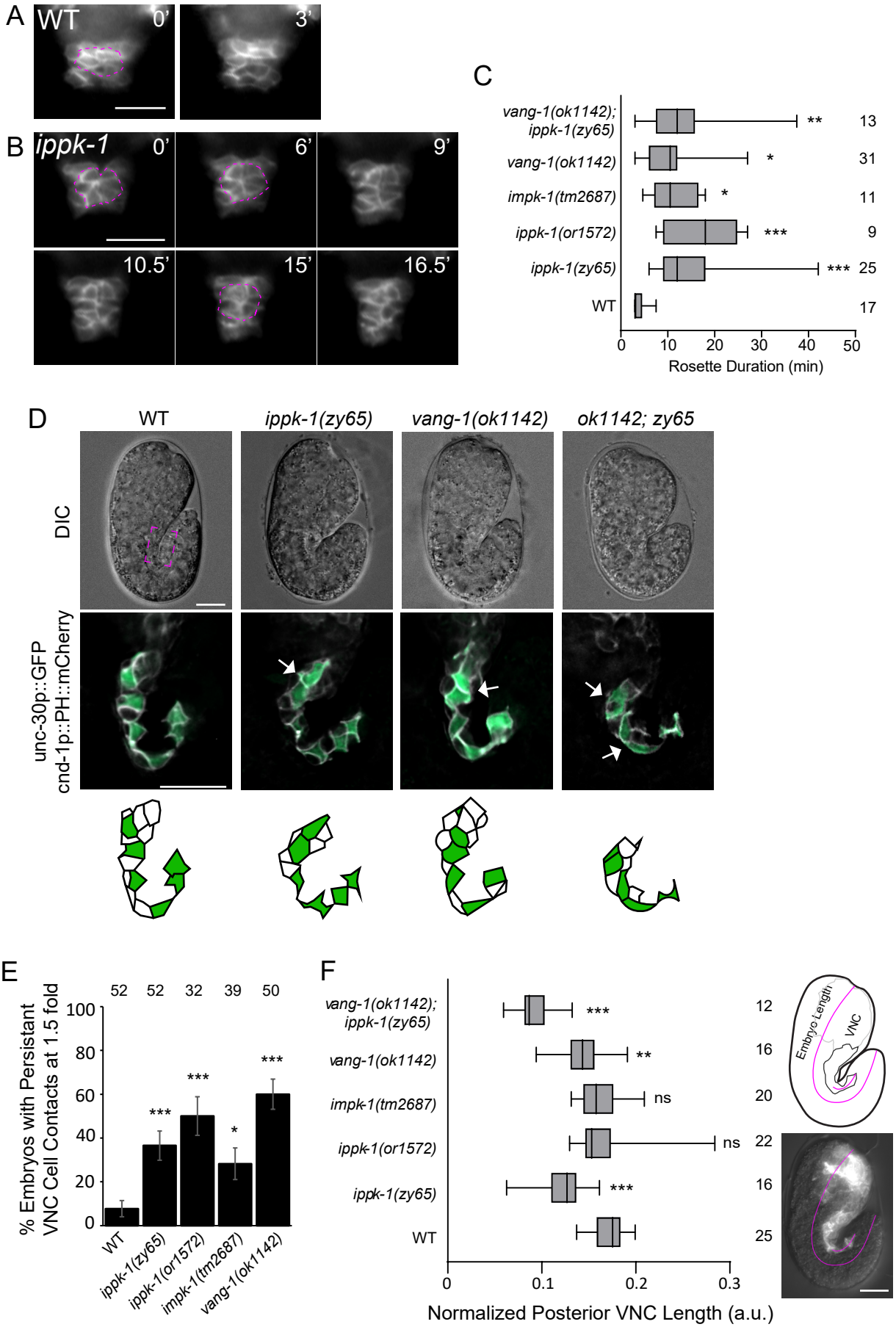
A
WT
0'
3'
B
ippk-1
0'
6'
9'
10.5'
15'
16.5'
C
vang-1(ok1142); ippk-1(zy65)
vang-1(ok1142)
impk-1(tm2687)
ippk-1(or1572)
ippk-1(zy65)
WT
**
*
*
***
***
13
31
11
9
25
17
0
10
20
30
40
50
Rosette Duration (min)
D
WT
ippk-1(zy65)
vang-1(ok1142)
ok1142; zy65
DIC
unc-30p::GFP
cnd-1p::PH::mCherry
E
52
52
32
39
50
100
80
60
40
20
0
% Embryos with Persistant VNC Cell Contacts at 1.5 fold
***
***
*
***
WT
ippk-1(zy65)
ippk-1(or1572)
impk-1(tm2687)
vang-1(ok1142)
F
vang-1(ok1142); ippk-1(zy65)
vang-1(ok1142)
impk-1(tm2687)
ippk-1(or1572)
ippk-1(zy65)
WT
***
**
ns
ns
***
12
16
20
22
16
25
0
0.1
0.2
0.3
Normalized Posterior VNC Length (a.u.)
Embryo Length
VNC

FIG 4

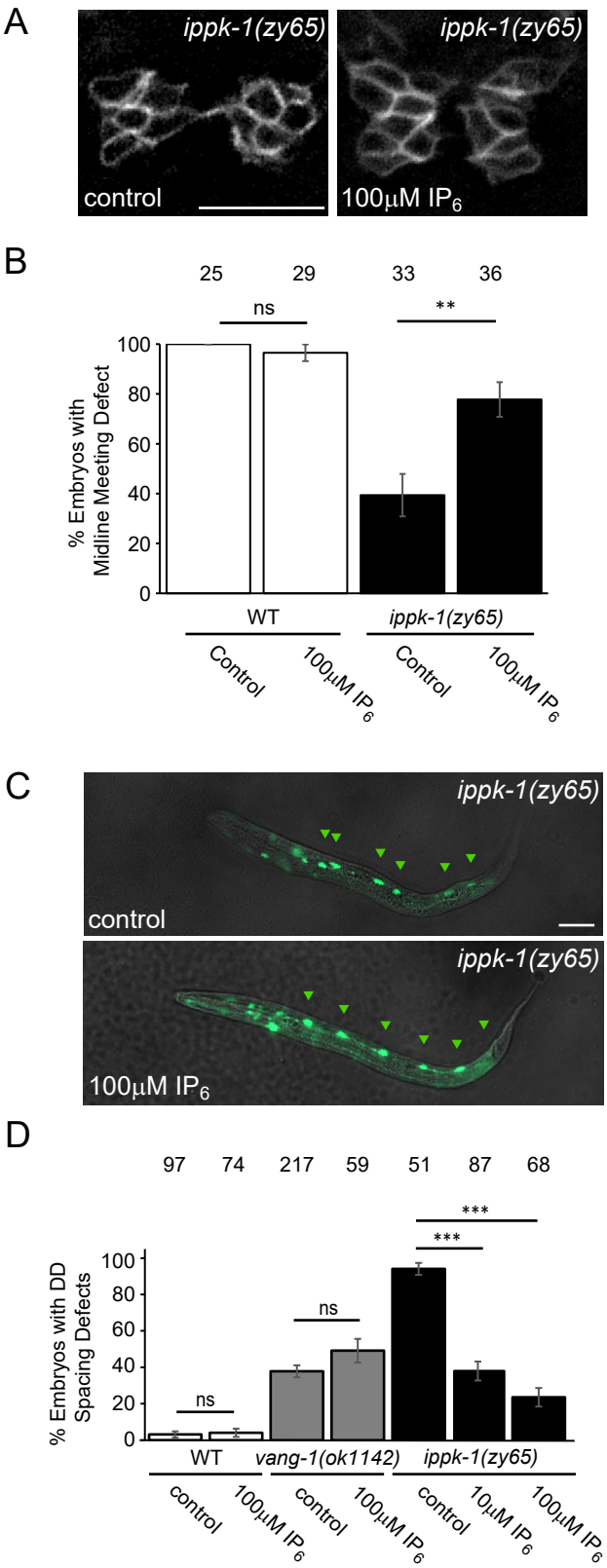
A
ippk-1(zy65)
control
ippk-1(zy65)
100μM IP6
B
25
29
33
36
ns
**
% Embryos with Midline Meeting Defect
100
80
60
40
20
0
WT
ippk-1(zy65)
Control
100μM IP6
Control
100μM IP6
C
ippk-1(zy65)
control
ippk-1(zy65)
100μM IP6
D
97
74
217
59
51
87
68
***
***
ns
ns
% Embryos with DD Spacing Defects
100
80
60
40
20
0
WT
vang-1(ok1142)
ippk-1(zy65)
control
100μM IP6
control
100μM IP6
control
10μM IP6
100μM IP6

FIG 5